Evaluation of Artificial Notches in Conductive Biomaterials by Sweep Frequency Eddy Current Testing

Milan Smetana, Daniela Gombarska, Filip Vaverka
Department of electromagnetic and biomedical engineering, Faculty of electrical engineering and information technology
University of Zilina
Univerzitna 1, 010 26 Zilina, Slovak Republic
milan.smetana@feit.uniza.sk

***Abstract*— Electromagnetic nondestructive evaluation of conductive biomaterials using the sweep frequency eddy current method is the subject of this work. The main aim is to verify its use in investigating artificial defects located inside the austenitic stainless steel. For this purpose, numerical simulations and experiments were carried out, which will be compared and evaluated.**

Keywords*— Sweep frequency eddy current testing, material defect, CST Studio Suite, eddy-current probe, harmonic excitation.

I. INTRODUCTION

The role of nondestructive evaluation of material structures is undeniable worldwide because it plays a significant role in the present time. Increased R&D activities in the field of NDE have been motivated by the need for precise evaluation of cracks and flaws to assess the expected life of mechanical components. Moreover, many industrial applications require complex inspection where the main aim is to prevent the failure of various parts [1], [2]. Periodic review of such elements and devices ensures their safe, effective, and long-term operation. New methods and devices are still being developed and designed to tackle gradually increasing demands for reliable detection and precise characterization of materials and their defects. NDE techniques are widely used in various industries to inspect multiple complex structures, such as biomaterials [3]. New technologies and activities from the last decades have allowed the design and development of particular types of sensors, which have properties suitable for electromagnetic NDE applications. The eddy current method (ECT) is theoretically well-known and widely utilized in practice. It is ideal for evaluating surface, subsurface, and near-surface defects, and it applies to almost all materials with non-zero conductivity. Some of the current innovations of the ECT account for increasing the information rate of sensed responses, especially new excitation techniques such as pulsed, chirp, and sweep-frequency. Other advances incorporate eddy current sensor arrays, flexible probes, and further probes with magnetic sensors such as Hall sensors, Fluxgate magnetometers, SQUID (Superconducting Quantum Interference Device) sensors, and GMR (Giant Magneto Resistance) sensors to detect small perturbation fields. The sweep frequency ECT method is a modification of a conventional ECT method. It is used in such cases where it is not possible to move the probe over the material under inspection [4], [5], [6]. This approach is based on the fixed location of the investigation at a concrete area, which is supplied by a harmonic signal. The frequency of the signal varies in discrete steps that are previously defined. The response signal is sensed in real time. This approach is based on the fixed location of the probe at a concrete place, which is supplied by a harmonic signal. The frequency of the signal varies in discrete steps that are previously defined. [7], [8], [9].

This study compares numerical simulations and experimental measurements of the SFECT method for defect detection ability and appropriate eddy current probe selection optimization.

II. NUMERICAL SIMULATIONS

The program CST Studio Suite is used to perform numerical simulations. CST Studio Suite is EM field problem-solving software. The program utilizes the finite element method (FEM) for the computation and analysis. A conductive structure is represented by the conductive material (austenitic stainless steel, grade AISI 316L) with the following geometry: width of w = 500 mm, length of l = 150 mm, and height of h = 10 mm. This material has a conductivity of 1 MS/m and a relative permeability equal to 1. The modeled material has isotropic properties. A cuboid-shaped inhomogeneity on the surface of the conductive structure, with zero conductivity, is present axially symmetrically in the middle of the design. The dimensions of inhomogeneity depend on the dimensions of inhomogeneities on the etalons used for the measurements. The dimension change is either for a single or both sizes at once. i.e., when the depth parameter d changes, length is constant at l_c = 10 mm, or if length l is changing, depth is constant at d_c = 5 mm, or both dimensions are changing together Fig. 1. The width is consistent for each crack. All defect dimensions are summarized in Table I.

A coil of an absolute-type surface probe generates the eddy currents. Three different types of EC probes are used. The first one is coreless (air-core probe, probe No.1), the second one has the presence of the ferrite core (Probe No.2), and the third one is a ferrite core and aluminum shield (Probe No.3). These probes consist of two coils: one is transmitting coil (Tx) and the second one is receiving coil (Rx). The Tx coil has several turns of N_{Tx} = 80, and the Rx coil's number of turns equals N_{Rx} = 140. The dimensions of all probes are shown in Fig. 2. In the SFECT approach, a probe in a static position is used without any movement above the inspected material. Three probe locations are used in the numerical simulation and for whole measurements: probe in the air, probe above the defect-free material as a reference, and

probe axially symmetrically above the material with the defect. A harmonic excitation signal with a magnitude of V_{pp} = 0.1 V and a frequency ranging from f = 1 kHz to f = 1.5 MHz, with a Δf = 10 kHz step, excites the transmitting coil in discrete steps.

TABLE I. THE GEOMETRY OF THE INSPECTED SPECIMENS

One parameter geometry change		Two parameters geometry change	
Depth [mm]	***Length [mm]***	***Depth [mm]***	***Length [mm]***
1	10	1	3
3	15	3	9
5	20	5	15
7	25	7	21
9	30	9	27

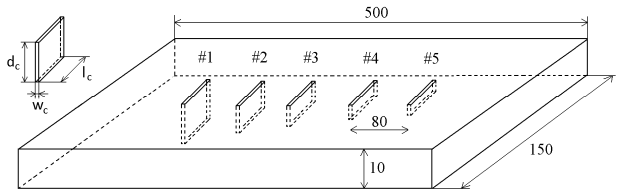

Fig. 1. The spatial configuration of the specimen with defects.

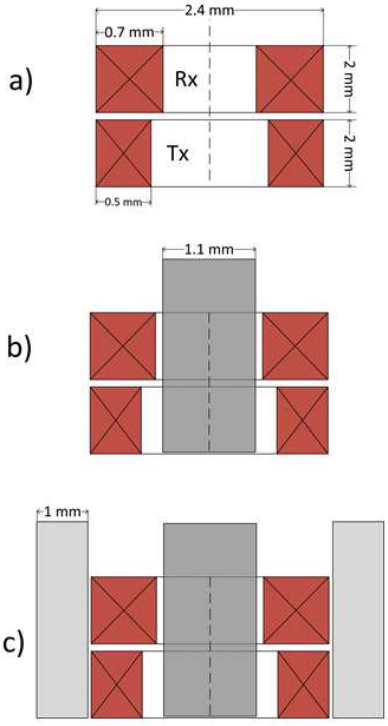

Fig. 2. Configuration and geometry of ECT probes: a) air-core probe, b) probe with ferrite core, c) probe with ferrite core and aluminum shield.

III. EXPERIMENTAL MEASUREMENTS

According to the numerical simulations, the measurements are carried out. Material etalons made of austenitic steel with artificial defects are used for measurements. The stainless austenitic steel used in these standards is designated as AISI 316L. The artificial defects were made using the electric discharge machining method. The flaws on the steel plates are the exact dimensions as those used in the simulations. The measurement probes are identical to the probes used in the simulation. An equal excitation signal and the same frequency interval drive the transmitting coil. Probes are in three different positions: in the air, above the material without the defect, and above the material with the artificial defect.

IV. NUMERICAL SIMULATION RESULTS

Values of induced voltage V on the Rx coil are acquired and processed from simulations and measurements. In simulations, the importance of the induced voltage VS for individual frequencies is obtained from the overall results of the simulation. During measurements, data gathering is more complex. A lock-in amplifier and LabVIEW are used to obtain the signal from measurement. Samples are received at a sampling frequency of f_s = 10 kHz for a time of sweeping one frequency t_s = 2 s. The output is the real and imaginary parts of the induced voltage, the averaged values from the samples. Matlab is used to connect these parts to a complex voltage V_M. The induced voltage values V_{Rx} are mathematically adjusted. The results of the induced voltage V_{Rx} in the air are subtracted from the other consequences for the obtained signal to depict the material's response to the excitation signal accurately. The response to the Tx coil is thus eliminated. The data are then normalized to the absolute value of the probe voltage in the air using the following equation:

$$V_{Rx} = (V_{Rx\text{-}defect} - V_{Rx\text{-}airt}) / (| V_{Rx\text{-}air} |) \quad (1)$$

where V_{Rx} [-] is the normalized voltage value, $V_{Rx\text{-}defect}$ [V] is the voltage of the coil over the defect or defect-free material, and $V_{Rx\text{-}air}$ [V] is the voltage of the coil in the air. After normalization, the absolute value and phase of the normalized induced voltage are calculated. These absolute values and phases are then plotted in graphs. These graphs are not the aim of this work but are informative. The purpose of this study is to compare simulation and measurement data. Therefore, the set of results is further statistically analyzed. First, the individual results of measurement are subtracted from the corresponding results of simulations, according to the equation:

$$\Delta V = (V_{Rx\text{-}Simulation} - V_{Rx\text{-}Measurement}) \quad (2)$$

where ΔV [-] is the difference, $V_{Rx\text{-}Simulation}$ [-] is the normalized voltage of the simulated coil, and $V_{Rx\text{-}Measurement}$ [-] is the normalized voltage of the measured coil. The difference ΔV between the two values is plotted and evaluated.

As mentioned above, the difference was plotted in three graphs for each probe. Fig. 3 shows the results of a coreless probe, Fig. 4 shows the results of a probe with a ferrite core, and Fig. 5 shows the results of a probe with a ferrite core and an aluminum cover. Each curve represents the differences between the simulated and measured data of the two parameters' geometry change. These results were chosen because they best represented the defects that can be detected in materials. The measurement results of the coreless probe and the ferrite core probe are more accurate than the core and shield probe, as shown in Fig. 1 and Fig. 2. The most significant difference was found around the frequency interval's edges, particularly at lower frequencies.

The same oscillation that occurred in the measurement results of probe 1 is responsible for the oscillation in Fig. 1. This oscillation was not random, as evidenced by all measurement data in [10]. Further investigation into its origin will be performed. Fig. 3 shows that adding an aluminum cover affects detection differently than the simulation predicted. Despite the widest difference between the simulated and measured data, probe No. 3 showed sufficient detection ability. Next, a statistical analysis was performed to evaluate the results better. On each statistical file, the median and standard deviation were calculated. The statistical set represented the results of individual coil geometry change differences. Table II. displays the results. The consistency of the differences is described by these results. It's possible to determine from them that, despite the oscillation, probe No. 1 performs the best. The average difference in Probe No. 2 is slightly higher. The worst results were from probe number three, which had a standard deviation of twelve to fourteen times that of Probe No.1.

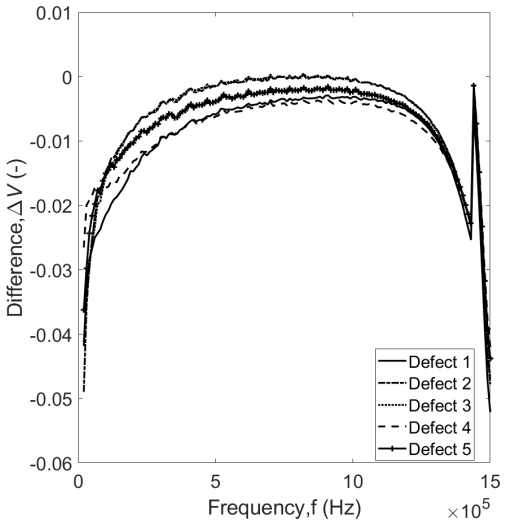

Fig. 3. Difference between simulation and measurement performed with probe No.1 on defects with two changing parameters.

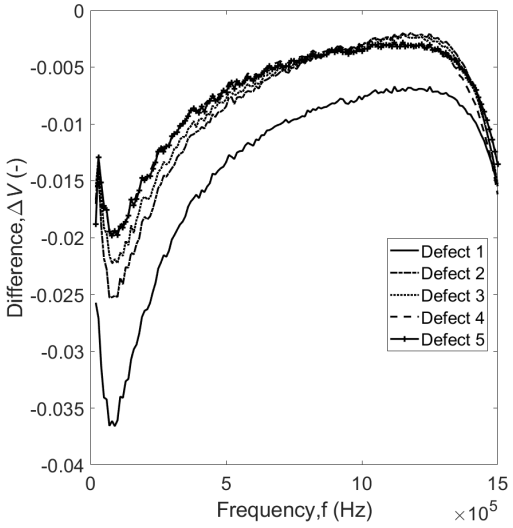

Fig. 4. Difference between simulation and measurement performed with Probe no.2 on defects with two changing parameters.

Calculating the standard deviation of the differences in the change in the dimensions of the defect for each frequency was another statistical study that was performed. The results are plotted in Fig. 6. The graph shows that for all probes in the frequency range of 50 kHz to 100 kHz, the standard deviation for individual changes in defect dimensions is the lowest. Furthermore, the graph demonstrates that Probe No. 1 produces the best findings again.

TABLE II. MEDIAN AND STANDARD DEVIATION OF DIFFERENCES

	Probe No.1		**Probe No.2**		**Probe No.3**	
	Med[a]	***STD***[b]	***Med***	***STD***	***Med***	***STD***
Depth	-0.0049	0.0079	-0.0059	0.0084	-0.028	0.1023
Length	-0.0043	0.0083	-0.0067	0.0254	-0.0467	0.1251
Two parameters	-0.0048	0.0101	-0.0072	0.0102	-0.0562	0.1437

[a.] Median.

[b.] Standard deviation

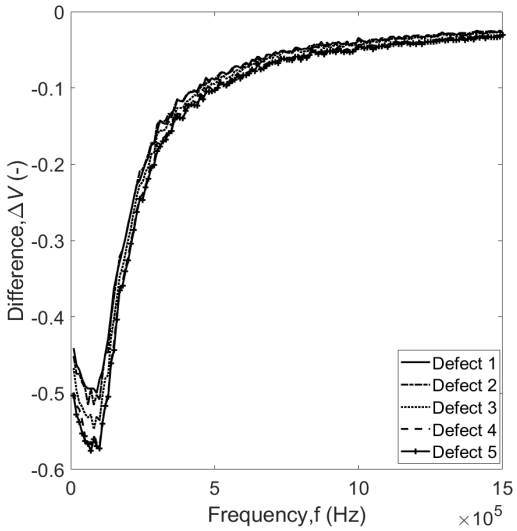

Fig. 5. Difference between simulation and measurement performed with Probe No.3 on defects with two changing parameters.

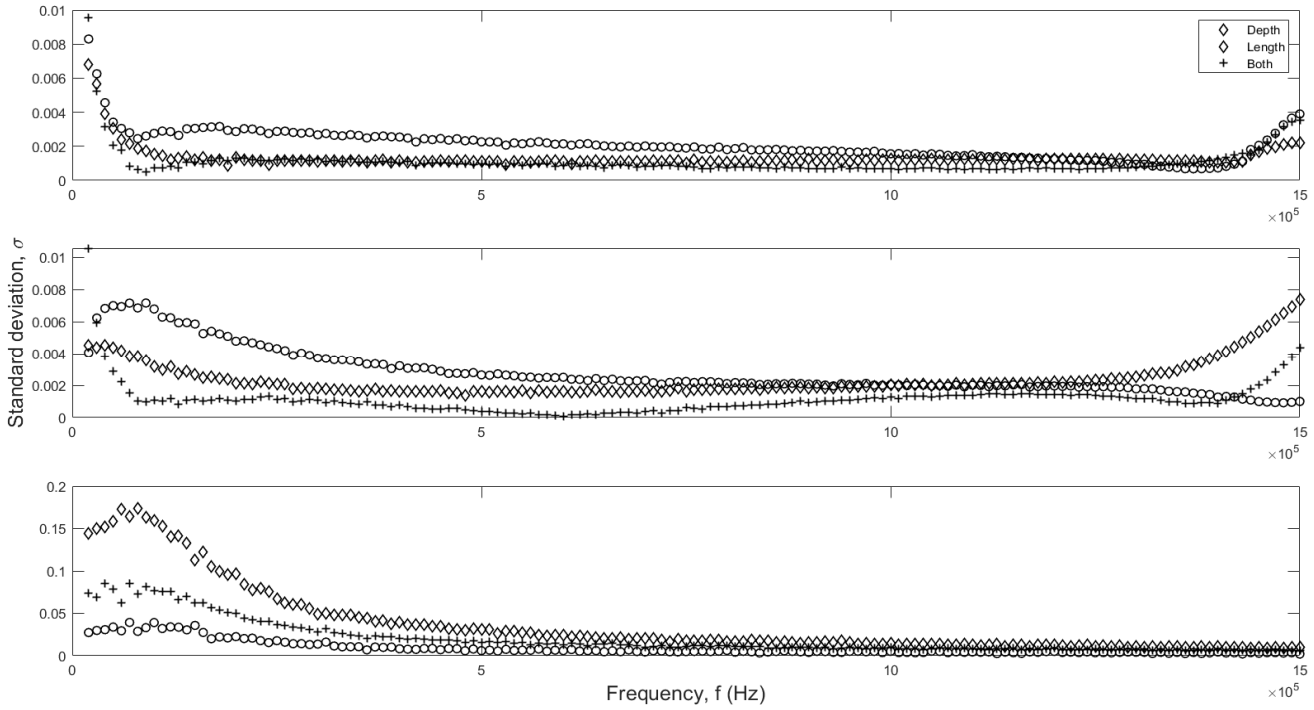

Fig. 6. Standart deviation of defect parameters differences according to the sweeping frequency.

V. Conclusion

The SFECT method is discussed in this article, as well as its use in electromagnetic non-destructive testing and investigation of conductive materials. The study compares numerical simulations and experimental measurements performed under the same conditions for various types of ECT probes. The measurements without a coreless probe correspond most closely to the results of simulations. The probe with core and cover compared to the results of the simulations at least. Although its measurement results were more promising for use in other SFECT NDT studies than the probe without the core. In the following studies, we will focus on the measurement of artificial defects and real defects with the most suitable investigation. Next, we will focus on adjusting the input parameters of the measurement, e.g., the frequency range of the excitation signal and the shape of the excitation signal.

Acknowledgment

This work was supported by the project APVV-19-0214.

References

[1] B.P.C. Rao, Practical Eddy Current Testing. Alpha industries International Ltd.J.2007.

[2] J. García-Martín, J. Gómez-Gil, and E. Vázquez-Sánchez, “Non-destructive techniques based on eddy current testing,” in Sensors, vol.11, 2011, pp. 2525-2565.

[3] R. Konar, M. Mician, M. Smetana, and V. Chudacik, “Real biomaterial evaluation by eddy current and ultrasonic inspection”, 2016 ELEKTRO, 2016, pp. 578-582.

[4] L. Janousek, A. Stubendekova, and M. Smetana.”Novel insight into swept frequency eddy-current non-destructive evaluation of material defects”, in Measurement, vol. 116, 2017, pp. 246-250.

[5] P. Karban, P. Kropík, V. Kotlan, and I. Doležel, “Bayes approach to solving TEAM benchmark problems 22 and 25 and its comparison with other optimization techniques”, in Applied Mathematics and Computation, vol. 319, 2018, pp. 681-692.

[6] L. T. Cung, T. D. Dao, P. C. Nguyen, and T. D. Bui, “A model-based approach for estimation of the crack depth on a massive metal structure” in Measurement & Control, vol. 51, 2018, pp. 182-191.

[7] W. Sriratana, Y. Khwankityotha and S. Satthamsakul, "Development of compatible induction coil with pure ac for hall effect sensor: A study on metal materials thickness," 18th International Conference on Control, Automation and Systems, 2018, pp. 575-579.

[8] A. Ribeiro, D. Pasadas, H. G. Ramos, and T. Rocha, ”Regularization of the Inversion Process in Eddy Current Characterization of Superficial Defects” in Proceedings of the 20nd International Workshop on Electromagnetic Non-destructive Evaluation, vol. 41, 2016, pp. 48-54.

[9] A. Duca, M. Rebican, L. Duca, L. Janousek, and L. Altinoz, “Advanced PSO Algorithms and Local Search, Strategies for NDT-ECT Inverse Problems”, in Journal of Scientific Computing, vol. 70, 2017, pp 29–59.

[10] F. Vaverka, M. Smetana, D. Gombarska, and L. Janousek, “Advanced PSO Algorithms and Local Search, Strategies for NDT-ECT Inverse Problems”, in Journal of Scientific Computing, vol. 70, 2017, pp 29–59.